Rapid Synthesis of Cesium Iodide Nanostructures

Elena Vasquez, Julian Styles
Max Planck Institute for Materials Science, Munich, Germany

***Abstract*—**This study presents how to use a high-efficiency process for producing cesium iodide (CsI) crystal columns by rapid heating method. In the past, the heating rate of the resistance wire heating furnace was relatively slow and excessive iodine and CsI vapors were therefore generated during heating. Because much iodine and CsI vapors are produced during heating process, the composition of CsI crystal columns is not correct. In order to enhance the heating rate, making CsI material in the heating process can quickly reach the melting point temperature. This study replaced the traditional type of external resistance heating furnace with halogen-type quartz heater, and then, CsI material can quickly reach the melting point. Eventually, CsI melt can solidify in the anodic aluminum template forming CsI crystal columns.

***Keywords*—**Cesium iodide, high efficiency, vapor, rapid heating, crystal column.

I. Introduction

THE scintillator material generates photons isotropically from the absorption of the X-rays [1], [2], and the photons can be imaged by the detector. The luminescence and scintillation characteristics of CsIs are widely used in the existing detectors [3]. By comparing the quantum noise and the threshold contrast of a human eye an upper limit for the sensitivity of an imaging system is determined [4]. CsI, which is used in the phosphor layer of a scintillator plate, exhibits a relatively high conversion rate of X- or γ -rays to visible light. An array of pores is etched into a silicon wafer, which is opaque to visible light [5], [6].

The scintillator can be directly coupled to a commercial charge-coupled device (CCD) and has the fastest response time (several ns) for real-time radiography. A high-performance detector based on a scintillating screen optically coupled to a CCD camera has been developed [7]. Individual sensor elements include a photosensor such as a photodiode or a phototransistor, and a conversion unit [8], [9]. CsI film has been one of the most extensively used scintillators for indirect X-ray imaging because of its needle-like micro-structure [10]. The conversion unit converts incident x-rays into low γ-energy radiation such as green light, for which the photo-sensors have a good sensitivity [11], [12].

In the conventional scintillation crystal fabrication techniques, an array of micron-tubes is often fabricated on a silicon wafer using deep reactive ion etching (DRIE) or laser drilling technologies. The depth of the micron tube can reach 20 to 25 μm, and the diameter is several tens of microns, and then, one can use liquid or gas phase methods to fill the CsI material into the micron tubes. However, the expensive equipment requirement and long process time increase the production cost.

In order to reduce the production cost and process complexity of scintillation crystals, the purpose of this article is to provide an ordering arrangement of CsI scintillation columns structure and a manufacturing method.

We suggest an anodic aluminum oxide as a candidate material for the CsI columns template. Aluminum anodization is probably the most controllable self-assembly process at lower cost. The anodized aluminum oxide (AAO) possesses unique features such as high aspect ratio, uniform pore size, and high structural ordering degrees. Additionally, it is stable in the chemical and thermal environment. The AAO is a type of ceramic with a high melting point (2072 °C) [13] and hardness (9 on the Mohs scale of mineral hardness) [14]. Anodic alumina has been named differently, such as anodic aluminum oxide (AAO), anodic alumina nanoholes (AAN), anodic alumina membrane (AAM), or porous anodic alumina (PAA) [15]. The anodic oxide film consists of two layers: the outer porous thick layer and the inner thin layer which is dense and dielectrically compact, and thus it is called as the barrier layer or dielectric layer.

II. Experimental Procedure

The procedure includes AAO fabrication, CsI nanoparticles form on the AAO inner pore wall, and a CsI column forms inside the AAO channel. The experimental procedure flow chart as shown in Fig. 1 including pre-treatment of aluminum substrate, AAO film formation, and CsI columns formation steps. First, in order to obtain a flat substrate, the high purity (99.999%) aluminum sheet was through (a) mechanical grinding, (b) stress release, and (c) electro-polishing steps. Following, a high quality AAO film included the fabrication steps of (a) first anodization, (b) remove anodic oxide, (c) second anodization, (d) remove Al substrate, (e) remove barrier layer, and (f) pore widening. Finally, the CsI columns formation in the AAO template also included the operation steps of (a) CsI nanoparticles on AAO pore wall, (b) CsI powder on AAO top surface, (c) heating, (d) CsI melt into AAO, and (e) cooling. The detail parameters of AAO template, CsI nanoparticles, and CsI column fabrication are discussed in the following.

AAO template: AAO templates with pore sizes of 10 to 500 nm were generated by anodizing a high purity aluminum (Al) substrate (99.999%) in acid solutions of sulfuric acid (H_2SO_4),

oxalic acid $(COOH)_2$, or phosphoric acid (H_3PO_4). The Al substrate was first ground to #2000 by SiC waterproof paper and then annealed in an air furnace at 550 ℃ for 1h. The sample was then electro-polished in a bath consisting of 15 vol.% perchloric acid, 70 vol.% ethanol, and 15 vol.% monobutylether with a charge of 42 V (DC) applied for 10 min, using a platinum plate as a counter. A 500 nm pore diameter template was then fabricated by anodizing the polished-Al substrate at 200 V in 1 vol.% H_3PO_4 at -3 ℃ for 1h, which was the first anodization. In order to obtain an orderly pattern on the substrate for the second anodization, the first anodization film was removed in 1.8 wt.% chromic acid (CrO_3) + 6 vol.% H_3PO_4 solution at 60 ℃ for 40 min [16]. The resulting substrate, with a regular pattern on the surface, was used for the second anodization for several hours to form AAO film with various thicknesses. Finally, the sample was put in 5 vol.% H_3PO_4 at 25 ℃ for 4h [17]. The nanotubes were widened to ordering pores.

CsI nanoparticles: In order to facilitate the CsI melt into the AAO template, CsI nanoparticles were first formed on the AAO inner pore wall by wet deposition method (1 wt.% CsI, at 25 ℃ for 3 min) and then the CsI nanoparticles were sintered in an atmosphere furnace (400 ℃ for 5 min).

CsI columns: The AAO sample with CsI nanoparticles adhered and CsI powder on the surface was put on a quartz slice first, and then the AAO sample/quartz combination was placed inside a rapid heating chamber and heated (650 ℃ for 1 min). Under these conditions, the CsI melt could then flow into the AAO template and solidify to CsI columns.

III. Results and Discussion

It is learned that the use of resistance wire heating takes more time to reach a specific temperature point. However, in the heating process, a large amount of CsI or iodine vapor also produced and escaped, resulting in waste of cesium raw materials. In order to improve the above problems, the CsI melt obtainment was by the rapid heating and pressure controlling process. In order to fill CsI melt into AAO template, a pressure controllable chamber is needed.

The ideas of fast and cost down of CsI/AAO include: fabrication of a large area and high thickness sub-micron tubular template by anodization method, and then filling CsI melt into template. The CsI melt can therefore solidify to a single crystal of sub-micron CsI column in the template. The CsI columns are expected to have a better X-ray image resolution at lower X-ray intensities.

Fig. 2 showed the schematic diagram of vacuum inhalation chamber. There are two rooms in the chamber and the pressure P_2 < pressure P_1. The CsI powder is set on the AAO template, and the heating template was controlled by the thermal couple and halogen-type quartz heater. When the temperature is higher than the CsI melting point, the CsI melt can penetrate into AAO channel assistance by the pressure difference between P_1 and P_2.

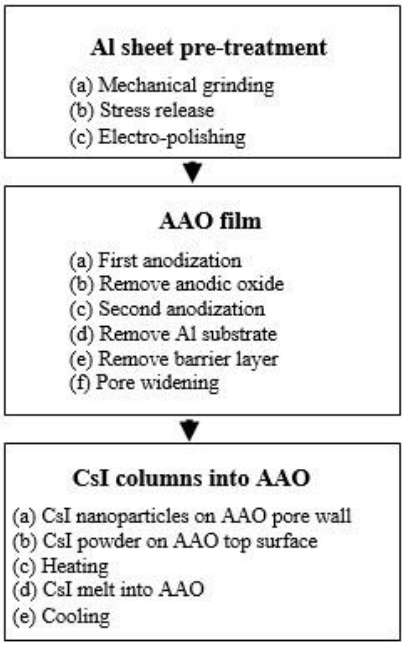

Fig. 1 Flow chart of experimental procedure

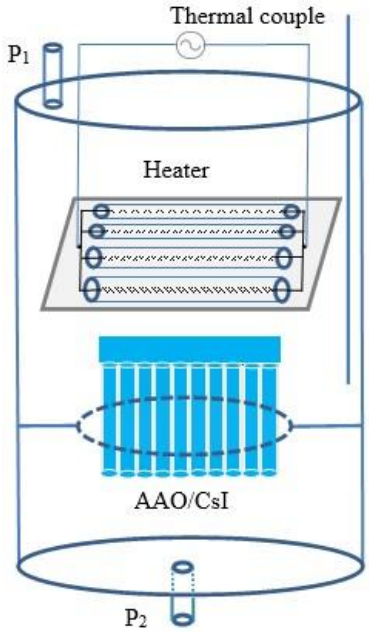

Fig. 2 Schematic diagram of vacuum inhalation chamber

Fig. 3 showed a detail exploded diagram of vacuum inhalation chamber. A vacuum heating chamber is filled in an inert gas and for placing a heating lamp and a thermocouple. A sample placement chamber is for the AAO/CsI sample setting. A vacuum tube-connected chamber is for connecting the vacuum pump and keeping the pressure in the vacuum state. Because of the pressures difference (P_2<P_1) between sample placement chamber (P_1) and a vacuum tube-connected chamber (P_2), it is more easily filling CsI melt into the AAO template. The clamps are for fixing the vacuum heating chamber, the sample storage chamber, and vacuum tube-connected chamber. The cooling ring is for protecting the O-ring

of soft gaskets. Fig. 4 showed the combination diagram of vacuum inhalation chamber.

The operation process or CsI melt into AAO template are following steps: (a) Placing the sub-micron channel of aluminum oxide template in the sample stage and placing a CsI sheet or powder (melting point: 621℃) on the aluminum oxide template. (b) The rapid heating chamber is heated to 650 ℃ by the halogen-type quartz heater and controled by the thermocouple.

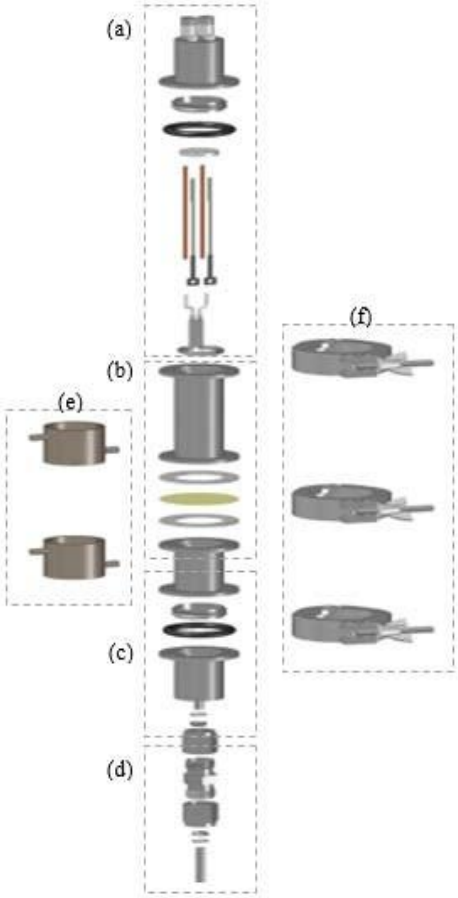

Fig. 3 The exploded diagram of vacuum inhalation chamber; (a) a vacuum heating chamber, (b) a sample placement cavity, (c) a vacuum chamber, (d) a vacuum connected group, (e) cooling rings, (f) clamps

The CsI compound has a sublimation point, melting point, and boiling point of 600 ℃, 627 ℃, and 1277 ℃ under 1 atm. Based on the physical properties of CsI, no vapors appear below 600 ℃ under 1 atm. However, when the CsI is heated in a pressure-controlled chamber, the vapor can be observed. In our experiment, a large quantity of vapor was clearly observed when the chamber pressure was higher than 1 atm.

Fig. 4 The combination diagram of vacuum inhalation chamber

In our previous calculation results [18], the thermodynamic stabilities of oxide compounds in a Cs-I-O system were evaluated by considering their Gibbs free energy. In ascending order of Gibbs free energy, the compounds in the temperature range of 25 to 800 ℃ are $Cs_2O_{(s)} \rightarrow Cs_2O_{(g)} \rightarrow Cs_2O_{3(s)} \rightarrow CsO_{2(g)} \rightarrow CsO_{(g)}$. Thus, $Cs_2O_{(s)}$ is the most stable phase, and $CsO_{(g)}$ is the least stable phase. Both $CsI_{(g)}$ and $I_{2(g)}$ vapors are formed below the $CsI_{(s)}$ melting point (627 ℃) at 1 atm; only $I_2(g)$, and no $CsI_{(g)}$ vapor, is formed below the CsI(s) melting point (627 ℃) at 1.15 atm; $CsI_{(g)}$ and $I_{2(g)}$ vapors do not form below the CsI melting point (627℃) above 213 atm. The thermodynamic calculations suggest that no vapors appear when the temperature is below 600 ℃.

In any electrolyte, higher anodizing voltages, lower electrolyte temperatures, and lower acid concentrations favor film growth. However, lower applied voltages, higher acid concentrations, and higher anodizing temperatures favor film dissolution [18], [19]. When the rate of film growth is equal to the rate of dissolution of the film in the electrolyte, the thickness of the film remains constant. There are many electrolytes and applied voltages used to produce AAO, and the most common are 10 vol.% sulfuric acid (18V), 3 wt.% oxalic acid (40 V), and 1 vol.% phosphoric acid (200 V) [20], [21], which are used to fabricate AAO with maximum pore sizes of 30 nm, 90 nm, and 500 nm, respectively [22].

Fig. 5 shows AAO images; (a) large size of AAO film, (b) AAO micro-structure, (c) side view of CsI filling in the AAO film, (d) zoom in CsI filling in the AAO film. It is easy to prepare a small sample of thin AAO film with nanosized pores. However, a large-area sample of AAO film with a submicron pore size and greater thickness is difficult to produce with a regular anodization process. In order to increase the CsI light emission efficiency and avoid cross-talk between CsI columns, we made a large size of AAO film with 480 nm pore size and thick film by using an anodization process and the electrochemical system of our design.

Fig. 5 AAO images; (a) large size of AAO film, (b) AAO micro-structure, (c) side view of CsI filling in the AAO film, (d) zoom in CsI filling in the AAO film

IV. CONCLUSIONS

In this paper, we provided a novel method of rapid heating for CsI columns fabrication. Because the CsI melt is confined to an AAO channel with a high aspect ratio, the melt easily solidifies into a stable single-crystal CsI column [23]. In this study, we combined the anodization and solidification technologies to fabricate single crystal CsI columns and that is a convenience and cost down process comparing to the DRIE or laser drilling technologies. The CsI columns are expected to have a better X-ray image resolution at lower X-ray intensities.

REFERENCES

[1] C.M. Schaefer-Prokop, D.W. De Boo, M. Uffmann, M. Prokop. DR and CR: Recent advances in technology, European Journal of Radiology, 72(2), (2009) 194-201.
[2] A. Koch, C. Raven, P. Spanne, A. Snigirev, X-ray imaging with submicrometer resolution employing transparent luminescent screens, Journal of the Optical Society of America A, 15(7), (1998) 1940-1951.
[3] S Zazubovich. Physics of halide scintillators, Radiation Measurements, 33(5), (2001) 699-704.
[4] A. M. Gurvich, Luminescent screens for mammography, Radiation Measurements, 24(4), (1995) 325-330.
[5] A Koch, H Rosenfeldt, Powder-phosphor screens combined with interference filters for X-ray imaging with increased brightness, Nuclear Instruments and Methods in Physics Research Section A: Accelerators, Spectrometers, Detectors and Associated Equipment, 432(2-3), (1999) 358-363.
[6] U.L. Olsen, X. Badel, J. Linnros, M. Di Michiel, T. Martin, S. Schmidt, H.F. Poulsen, Development of a high-efficiency high-resolution imaging detector for 30–80 keV X-rays, Nuclear Instruments and Methods in Physics Research Section A: Accelerators, Spectrometers, Detectors and Associated Equipment, 576(1), (2007) 52-55.
[7] M. Stampanoni, G. Borchert, P. W., R. Abela, B. Patterson, S. Hunt, D. Vermeulen, P. Rüegsegger, High resolution X-ray detector for synchrotron-based microtomography, Nuclear Instruments and Methods in Physics Research Section A: Accelerators, Spectrometers, Detectors and Associated Equipment, 491(1-2), (2002) 291-301.
[8] A. Ananenko, A. Fedorov, A. Lebedinsky, P. Mateychenko, V. Tarasov, Y. Vidaj, structural dependence of CsI(Tl) film scintillation properties, Semiconductor Physics, Quantum Electronics & Optoelectronics, 7(3), (2004) 297-300.
[9] E. Zych, C. Brecher, and H. Lingertat, Depletion of high-energy carriers in YAG optical ceramic materials, Spectrochimica Acta Part A: Molecular and Biomolecular Spectroscopy, 54(11), (1998) 1771-1777.
[10] B.Z. Zhao, X.B. Qin, Z.D. Feng, C.F. Wei, Y. Chen, B.Y. Wang, L. Wei, Performance evaluation of CsI screens for X-ray imaging, Chinese Physics C, 38 (11), (2014) 116003.
[11] H. Imai, Y. Takei, K. Shimizu, M. Matsuda, and H. Hirashima, Direct preparation of anatase TiO_2 nanotubes in porous alumina membranes, Journal of Materials Chemistry, 9(12), (1999) 2971-2972.
[12] H. Imai, M. Matsuta, K. Shimizu, H. Hirashima, N. Negishi, Preparation of TiO_2 fibers with well-organized structures, Journal of Materials Chemistry, 10, (2000) 2005-2006.
[13] G.C. Wood, J.P. O'Sullivan, The Anodizing of Aluminum in Sulphate Solutions, Electrochim. Acta, 15 (1970) 1865-1876.
[14] H. Xing, L. Zhiyuan, W. Kai, L. Yi, Fabrication of Three Dimensional Interconnected Porous Carbons from Branched Anodic Aluminum Oxide Template, Electrochem. Comm., 13 (2011) 1082-1085.
[15] C.C. Chen, D. Fang, Z. Luo, "Fabrication and Characterization of Highly-Ordered Valve-Metal Oxide Nanotubes and Their Derivative Nanostructures", Review in Nanoscience and Nanotechnology 1, (2012) 229-256.
[16] C.C. Chen, J.H. Chen, C.G. Chao, "Post-treatment Method of Producing Ordered Array of Anodic Aluminum Oxide Using General Purity Commercial (99.7%) Aluminum, Jpn. J. Appl. Phys. 44, (2005) 1529-1533.
[17] S.H. Chen, C.C. Chen, Z.P. Luo, C.G. Chao, "Fabrication and characterization of eutectic bismuth-tin (Bi-Sn) nanowires", Materials Letter 63, (2009) 1665-1668.
[18] S.H. Chen, C.C. Chon C.G. Chao, "Novel Morphology and Solidification Behavior of Eutectic Bismuth-Tin (Bi-Sn) Nanowires", J. Alloys Compd. 481, (2009) 270-273.
[19] W.C. Say, C.C. Chen, "Formation of Tin Whiskers and Spheres on Anodic
Aluminum Oxide Template", Jpn. J. Appl. Phys. 46, (2007) 7577-7580.
[20] C.Y. Chen, C.W. Hun, S.F. Chen, C.C. Chen, J.S. Lin, S.S. Johnson, N. Noel, N. Juliely, Z.P. Luo, "Fabrication of Nanoscale Cesium Iodide (CsI) Scintillators for High-Energy Radiation Detection", Review in Nanoscience and Nanotechnology, 4 (2015) 26-49.
[21] C.G. Kuo, C.C. Chen, "Technique for Self-assembly of Tin Nano-particles on Anodic Aluminum Oxide (AAO) Templates", Materials Transactions 50, (2009) 1102-1104.
[22] J.S. Lin, S.H. Chen, K.J. Huang, C.W. Hun, C.C. Chen, Challenges to Fabricate Large Size-Controllable Submicron Structured Anodic-Aluminum-Oxide Film", Atlas Journal of Materials Science, 2 (2015) 65-72.
[23] C.Y. Chen, S.H. Chen, C.C. Chen, J.S. Lin, Using Positive Pressure to produce a Sub-micron Single-Crystal Column of Cesium Iodide (CsI) for Scintillator Formation, Materials Letters, 148 (2015) 138-141.